Ceramics International 48 (2022) 10164–10173

Contents lists available at ScienceDirect

Ceramics International

journal homepage: www.elsevier.com/locate/ceramint

Green and cost-effective synthesis of zinc oxide thin films by L-ascorbic acid (AA) and their potential for electronics and antibacterial applications

Abdulkadir Taşdemir [a], Nazife Akman [b], Abdullah Akkaya [c,*], Raşit Aydın [d], Bünyamin Şahin [e]

[a] Department of Biology, Faculty of Science, Erciyes University, Kayseri, Turkey
[b] Vocational College, Kapadokya University, Nevşehir, Turkey
[c] Mucur Vocational School, Tech. Prog. Department, Kırşehir Ahi Evran University, Kırşehir, Turkey
[d] Department of Physics, Faculty of Sciences, Selcuk University, Konya, Turkey
[e] Department of Physics, Faculty of Arts and Sciences, Hatay Mustafa Kemal University, Hatay, Turkey

ARTICLE INFO

Keywords:
Zinc oxide
Nanoparticles
L-ascorbic acid
Green synthesis
Antibacterial properties

ABSTRACT

The evolution of eco-friendly, green route and cheap technology for synthesizing nanostructured zinc oxide (ZnO) thin films using plant extracts is a promising choice because such materials present a widespread potential for numerous technological applications. This study proposes the green and cost-effective technique to synthesize stable ZnO thin films using a good reducing agent and facilitating many natural L-ascorbic acids (AA) metabolic reactions capacity. The influence of AA concentrations in the starting bath solution on ZnO samples' structural, morphological, electrical and antibacterial performances has been reported in detail. The main physical characteristics of the ZnO materials were improved by supplementing of reducing and capping agents AA. Average particle size varies with the adding AA from 58.29 to 48.68 nm and also thickness of these films was decreased from 0.82 to 0.44 μm. Also, it was seen that, the presence of AA in the bath solution significantly affected the absorption process and causes a morphological alteration due to the reaction between Zn^{2+} and AA during the deposition process. FTIR transmittance spectra of bare ZnO presented that a transmittance peak about 886 cm^{-1} and 748 cm^{-1} was created by the characteristic stretching vibration mode of the Zn–O. The resistivity of the produced films significantly changed with AA concentration in the bath solution. Antibacterial potentials of bare ZnO and ascorbic acid added ZnO films were examined against economically important *Staphylococcus aureus* (ATCC 25923) gram-positive bacteria and *Escherichia coli* (ATCC 35218) gram-negative bacterial disease agents via handling paper disc diffusion assay. The obtained diameter of the zones of inhibition was 20.1 mm for *E. coli* and 28.1 mm for *S. aureus* at the dose of ZnO+AA 8.0%. These inhibition diameters were larger than the diameter of ampicillin as our positive control alone. This proves that the newly synthesized compound is a powerful antibacterial agent.

1. Introduction

In the last ten years, zinc oxide (ZnO) nanofilms have invited attention because of their attractive physical characteristics and potential optoelectronic device applications. ZnO is one of the influential group II-VI compound metal oxide materials. The natural crystal morphology of ZnO is the hexagonal wurtzite structure, with lattice constants a = 3.25 Å and c = 5.12 Å. It is also a non-toxic, inexpensive, and naturally n-type semiconducting material with a room temperature direct and wide optical energy band gap of 3.37 eV [1–6]. Due to its excellent performance in optics, electronics, and photonics, the manufacture of ZnO films has been a practical area for their commercial applications in transducers, solar cells, catalysts, optical waveguides, UV-light emitters, photodetectors, lasers, and photodiodes [2–7].

A large number of fabrication techniques, such as sol-gel, thermal decomposition, sol-gel, pulsed laser deposition, sputtering, hydrothermal, precipitation, vapor phase oxidation, and successive ionic layer adsorption and reaction (SILAR) methods, have been used to synthesize high-quality ZnO thin films [8–15]. SILAR has the crucial advantages of economy, simplicity, flexibility, and easy control of deposit parameters among these different growth procedures. It requires neither a sophisticated instrument nor a vacuum system [16–18].

At present, a green attempt is preferred due to its reliability and sustainability compared to other standard synthesis methods. AA acts as

* Corresponding author.
E-mail address: abdullah.akkaya@ahievran.edu.tr (A. Akkaya).

https://doi.org/10.1016/j.ceramint.2021.12.228
Received 8 September 2021; Received in revised form 11 December 2021; Accepted 22 December 2021
Available online 25 December 2021

a capping and reducing agent for the synthesis of metal oxide nanostructures. AA molecules can enclosure the crystalline structure and intercept the uncontrolled growth of the particle size and distributions. Furthermore, the physical characteristics of the thin film materials can be improved by supplementing reducing and capping agents in the growth bath.

Ascorbic acid is very similar in molecular structure to glucose; it is the enolic form of alpha ketolactone. A set of compounds showing the biological activities of AA is commonly referred to as vitamin C. Except for primates, guinea pigs, and fruit bats, most mammals can synthesize vitamin C from glucose. Ascorbic acid is absorbed in the distal part of the small intestine up to 100 mg per day [19]. Significant dietary sources of vitamin C are red pepper, citrus fruits, tomatoes, cabbage, Brussels sprouts, cauliflower, strawberries, and spinach [20].

Ascorbic acid is a biological electron donor agent that enables certain enzymes to perform their activity. Blood concentrations of AA are arranged by renal excretion; dehydroascorbic acid enters erythrocytes and leukocytes by passive transport [24]. The pituitary, adrenal, brain, leukocytes, and eye have the highest quantities of AA [25]. Due to this feature, it has a robust antioxidant capacity [21]. The main functions of AA are fatty acid transport, collagen synthesis, neurotransmitter synthesis, and the prevention of oxidative damage to DNA [22–27]. The most specific symptoms of AA deficiency are scurvy, follicular hyperkeratosis, Sjögren's syndrome, ecchymoses, gingivitis, perifollicular hemorrhage with petechiae and anemia [28].

One of the most important causes of community-acquired and health-related bacteremia is *S. aureus*. The annual incidence of *S. aureus* bacteremia (SAB) in the United States is between 38.2 and 45.7 per 100000 people per year [29–31] and leads to two to ten deaths per 100 000 population per year globally [32]. Also, annual mortality rates for *E. coli* bacteremia ranged from 2.9 to 10.3 per 100 000 persons [33]. The yearly cost of average microbial resistance, which causes 33000 deaths in Europe and 29500 deaths in America, is approximately 1.5 billion dollars per year for European countries [19]. CLSI and EUCAST have stated that *E. coli* (ATCC 35218) and *S. aureus* (ATCC 25923) strains can be used in antimicrobial studies [34,35].

It has become imperative to take precautions against increasing antibiotic resistance. Although there are studies on the antimicrobial properties of AA, whose antioxidant properties are well known, they are not sufficient. Furthermore, investigations on the green synthesis of nanomaterials with AA are still limited [35–43]. The re-synthesis of vitamins and ZnO as nanomaterials can provide us with new weapons in fighting antibiotic-resistant bacteria to benefit from the synergistic effect. Green and cost-effective synthesized nanostructured materials for this purpose are very significant for exploring alternative ways.

Because of this reason, in this research, synthesis, and characterization of zinc oxide thin films by L-ascorbic acid via SILAR technique and their potential application for electronics and antibacterial have been recorded. Our goal is to manufacture nanosized ZnO-based thin films with enhanced structural, morphological electrical, and elevated antibacterial properties. The obtained consequence exhibited that AA concentration in the bath solution displayed an influential role in the main physical properties and antibacterial effectiveness of ZnO thin films.

2. Experimental procedure

2.1. Green synthesizing procedure of nanostructured ZnO

All the chemicals used in these syntheses were of analytical reagent grade and were procured from Sigma-Aldrich, USA. Zinc acetate dihydrate ($Zn(CH_3COO)_2$-$2H_2O$) and L-ascorbic acid ($C_6H_8O_6$) were used as Zn^{2+} ion source and reducing agent respectively. Also, in all experiments, acetone, diluted sulfuric acid and pure water were used to clean glass slides and beakers. The nanostructured ZnO films with and without AA ($C_6H_8O_6$) were grown using the SILAR route on a soda-lime glass substrate (Fig. 1). A sufficient amount of zinc acetate dihydrate ($Zn(CH_3COO)_2$-$2H_2O$) was added to deionized (DI) water to get a 0.15 M zinc acetate growth solution bath. Then, the solution was stirred at room temperature for 30 min in a magnetic stirrer to obtain a homogeneous synthesis mixture. The pH value of the growth bath was reached at around 10.0 by using ammonium hydroxide (NH_4OH). The pre-cleaned soda-lime glass substrates were dipped into the zinc acetate growth bath solution for 25 s (70 °C) and then rinsed with DI water (70 °C) for another 25 s removing the loosely bounded ions on the substrates. These dipping cycles were repeated 30 times to acquire good quality uniform thin films of nanostructured ZnO. The possible chemical reactions of ZnO films based on the SILAR deposition process can be summarized as follows [44,45];

$$Zn(CH_3COO)_2 + 2NH_4OH \rightarrow Zn(OH)_2 + 2CH_3COONH_4$$

$$Zn(OH)_2 \rightarrow ZnO + H_2O$$

Meanwhile, AA was supplemented to the growth bath, Zn^{2+} ions interacted with AA. Zn^{+2} ions can electrostatically interplay with $C_6H_8O_6$ ions. This process can be specified as given below [44–46];

$$Zn^{2+} + C_6H_8O_6 \rightarrow Zn + C_6H_6O_6 + 2H^+$$

Two series of samples (the volume proportion of L-ascorbic acid powder are 0%, 4.0%, and 8.0%, respectively) were prepared to investigate the impact of different concentrations of L-ascorbic acid powder in the zinc acetate bath as a green additive on ZnO thin samples. Finally, the grown ZnO thin film and powders were annealed at 50 °C for 180 min.

TLM patterns were fabricated by using a tungsten mask technique. The Au contacts were evaporated thermally in NANOVAK-NVTS 400 evaporation system, and thickness was 150 nm. During the Au evaporation process, background pressure was better than $1x10^{-6}$ Torr, and the deposition rate was 1–1.2 nm/s.

2.2. Characterizations of nanostructured ZnO

The morphological characterization of the ZnO films was done with a scanning electron microscope (SEM) and SEM- Evo Ls 10, Carl Zeiss NTS. The chemical composition was determined by using energy-dispersive X-ray spectroscopy (EDX). The crystal structure of the ZnO samples was carried out by X-ray diffraction (A Bruker D8 Advance X-ray diffractometer) by the use of Cu Kα radiation (λ = 1.5418 Å). The thickness of ZnO films was determined using a surface profilometer (AEP Technology, NanoMap 500LS 3D). The infrared spectrum of the ZnO films was obtained by a Fourier transform infrared (FTIR) spectrometer (Vertex 70v FTIR Spectrometer-Bruker). I-V measurements were executed by using a computer-controlled Agilent B2912A SMU at room condition and in the dark. Recording and calculations of data were conducted via SeCLaS software [47,48].

2.3. Preparation of Staphylococcus aureus (ATCC 25923) and Escherichia coli (ATCC 35218) strains and antibacterial responses of nanostructured ZnO

We used the agar disk diffusion method, one of the most flexible susceptibility testing methods to perform antimicrobial examinations of nanosized ZnO materials. Gram-positive *S. aureus* (ATCC 25923) and gram-negative *E. coli* (ATCC 35218) bacterial strains approved by EUCAST for antibacterial studies were selected as test microorganisms. For resuscitation, bacterial strains were first inoculated onto Blood agar (Merck, Germany). Colonies of the strains were inoculated on Tryptic Soy Agar (TSA) (Merck, Germany) after overnight incubation, and antimicrobial studies were performed for each species in the TSA. Each bacterial suspension was inoculated in 0.9% saline solution at 0.5 McFarland ($1x10^8$ cells per/ml) standard density. The prepared

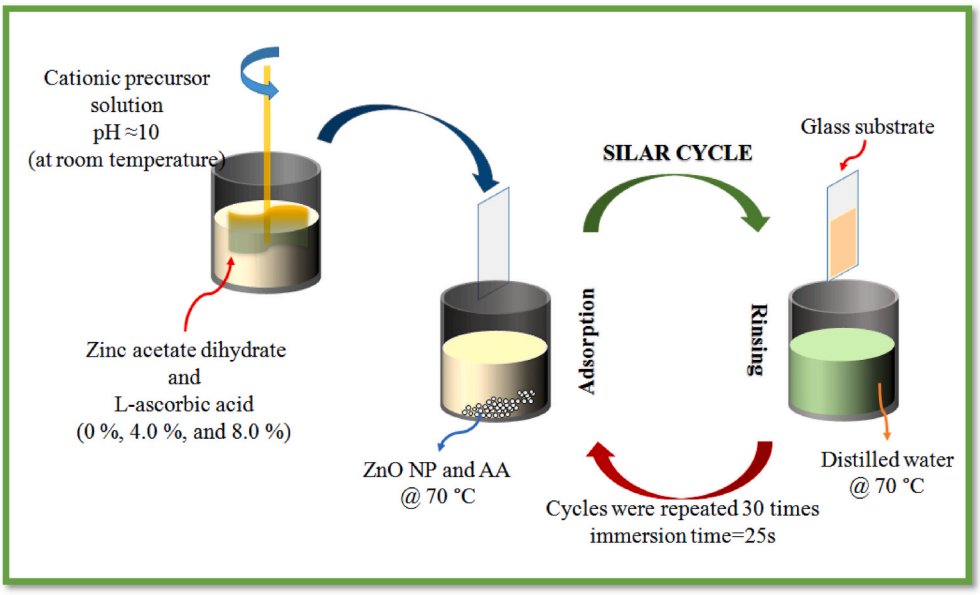

Fig. 1. Schematic illustration of experimental setup of SILAR procedure for deposition of AA added ZnO films.

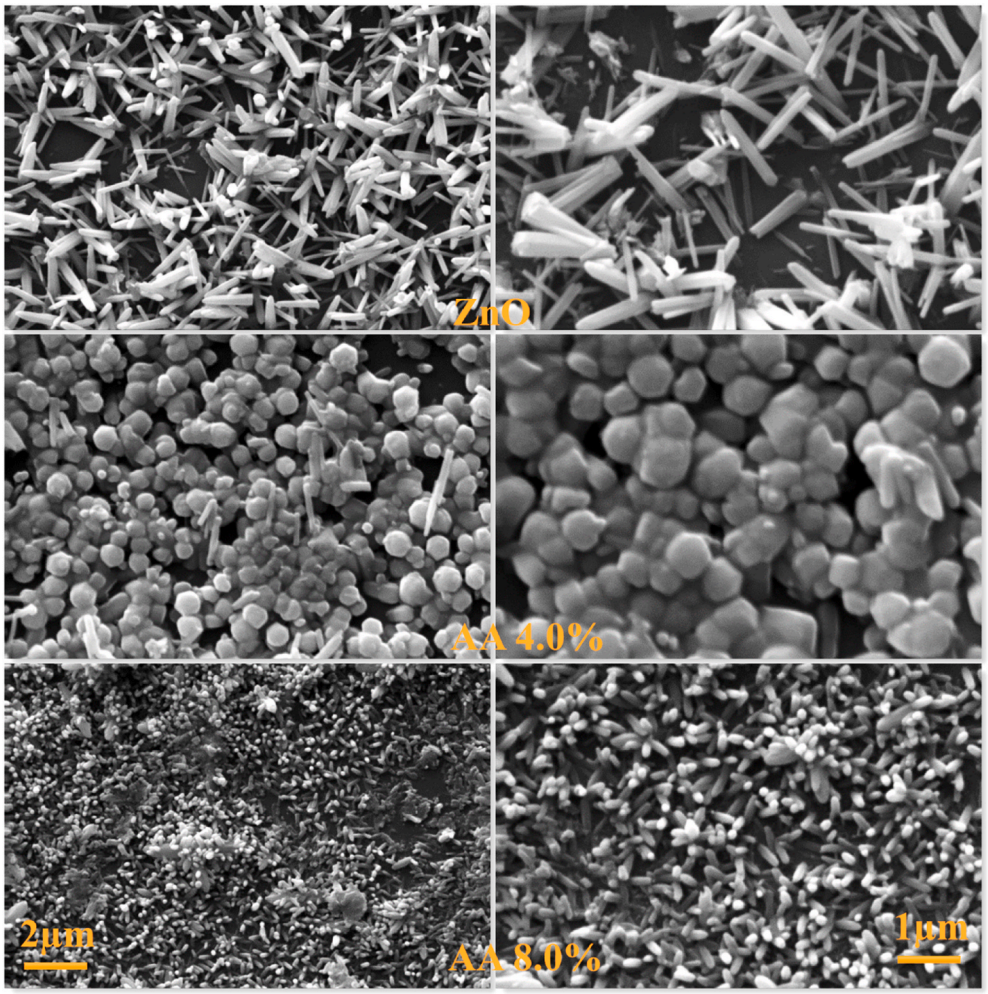

Fig. 2. SEM images of ZnO thin films as a function of AA concentrations. It can be seen that the bare ZnO has a rod-like structure. With the introduction of AA to the reaction bath, the surface structure of the ZnO sample changed intensely.

bacterial suspension overlaid the Mueller-Hinton (Becton Dickinson; USA) agar surface by sterile swab. Six discs (6 mm) were placed in each Petri dish. Standard antibiotic discs (ampicillin) were placed in the middle of the Petri dishes as positive controls. The bare ZnO, ZnO+AA 4.0% and ZnO+AA 8.0% were solved (mg/mL) in 10% dimethyl sulfoxide (DMSO) (Merck, Germany). Microorganisms were kept at 37 °C for 24 h in the incubator. An electronic caliper is used for determining the diameters of the inhibition zones.

3. Results and discussions

3.1. Surface morphological analysis of nanostructured ZnO

Microstructural properties on nanostructured ZnO films with and without AA as a reducing agent were carried out by SEM. The SEM photographs of the ZnO nanoparticles obtained with various concentrations of AA are presented in Fig. 2, from which it is observed that the bare ZnO has a rod-like structure. With the introduction of AA to the reaction bath, the surface structure of the ZnO sample changed intensely. If AA is added to the solution bath at a 4.0% concentration, sphere-like ZnO structures are observed, as indicated in Fig. 2. While the content of AA 8.0% had increased, the shape of nanoparticles transferred to a rod-like structure, owing to the impact of AA. The reason for the morphological alteration is the reaction between Zn^{2+} and AA during the deposition process. After the nucleation, AA may influence the particle morphological structure [49–51]. Fig. 3 indicates that magnified SEM images of ZnO films with various concentrations of reducing agent like AA. Measured mean values of the particle thickness were found to be 134.5, 707.5 and 142.3 nm for the ZnO films without AA, 4.0 and 8.0% AA contents in the growth bath, respectively. It can be seen in Fig. 3 that, the particle thickness of the ZnO films changed with the AA concentrations. The reason for the particle thickness alteration is the reaction between Zn^{2+} and AA during the deposition procedure. The results of the EDX point analysis from the ZnO sample are shown in Fig. 4, where the presence of Zn and O is confirmed from EDX analysis.

3.2. Structural analysis of nanostructured ZnO

The structural characterization of ZnO film with and without AA as a reducing agent is examined by the X-ray diffraction (XRD) technique. The XRD plots of the as-synthesized products using various AA concentrations by the SILAR method are displayed in Fig. 5. From the XRD analysis, it is observed that all the diffraction patterns are well matched with the standard hexagonal wurtzite structure of ZnO corresponding to the JCPDS card (File No. 0 01-075-6445) [52]. Three dominant diffraction peaks at 2θ value 32.19°, 34.87°, and 36.65°, correspond to the crystal lattice planes of (100), (002), and (101), respectively. No characteristic diffraction peaks of other impurities were observed in the XRD patterns. The intense and sharp diffraction peaks indicate well crystallinity of the deposited films. As the concentration of AA was increased from 4.0% to 8.0%, the intensity of the (100) diffraction peak decreased gradually. The reduction in the peak intensity may be due to the synergistic effect of AA as a reducing agent. From this, it is understood that the change in the AA content of the reaction bath has a significant effect on the crystallinity of the ZnO films [53,54].

To compute the mean crystallite size of the ZnO films, the Debye-Scherrer rule was used [55–57].

$$D = \frac{K\lambda}{\beta cos\theta} \quad (1)$$

In this equation, D is crystallite size, K is the Scherrer constant (equal to 0.94), β is the full-width half-maximum measured in radiations, and θ is the Bragg's diffraction angle. The estimated crystallite sizes of ZnO nanoparticles are highlighted in Table 1. The average D for ZnO films is 58.29, 50.41, and 48.68 nm, respectively. Table 1 clearly illustrates that crystallite size decreases with adding AA compared with bare ZnO film

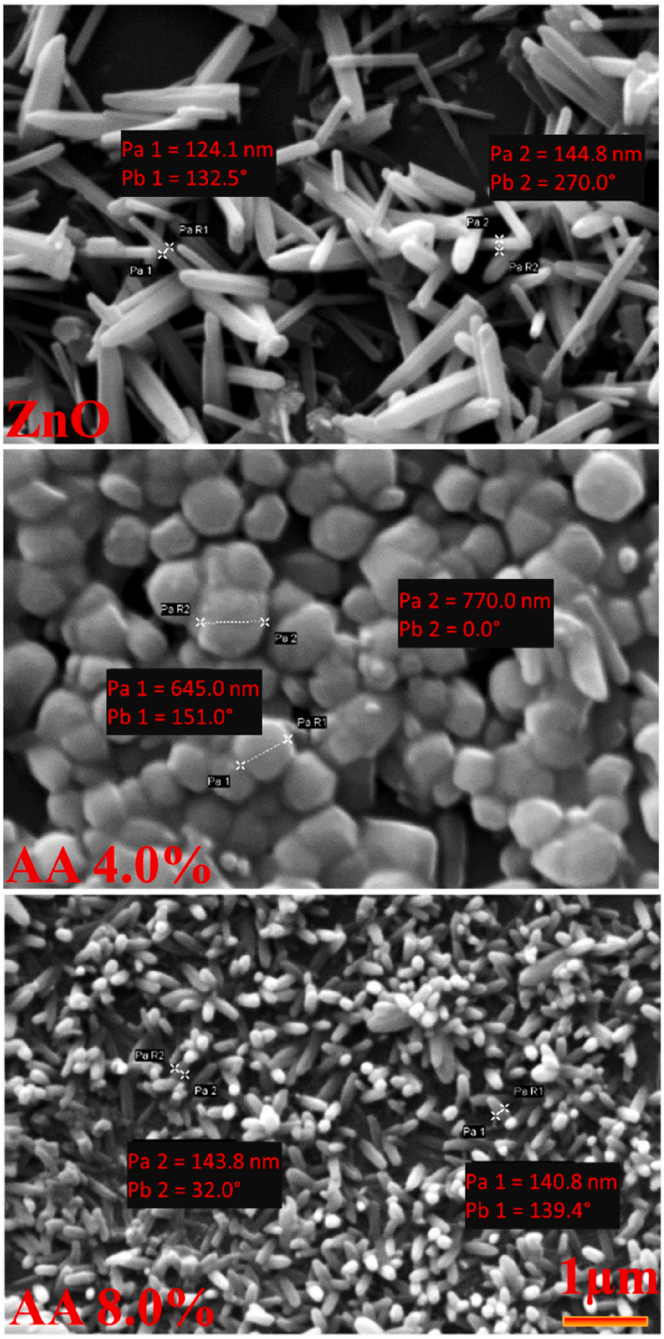

Fig. 3. Magnified SEM images of ZnO films with various concentrations of AA.

[58,59]. The thickness of these films is outlined in Table 1. It can be seen that the AA concentration increases from 0.0% to 8.0% as the film thickness decreases from 0.82 to 0.44 μm. The capping and reducing agent like AA are significant materials that can affect the degradation speed and hereby crystallinity quality and particle morphology. The degradation ability the capping and reducing agents may reason a change in the nucleation and growth kinetics of nanostructured metal oxide materials [52,60].

3.3. FTIR analysis of nanostructured ZnO

Fig. 6 shows the FTIR transmittance spectra of bare ZnO and AA added ZnO films. In the spectrum of bare ZnO, it can be seen that a transmittance peak emerged at about 886 cm^{-1} and 748 cm^{-1} created by the characteristic stretching vibration mode of the Zn-O. It was

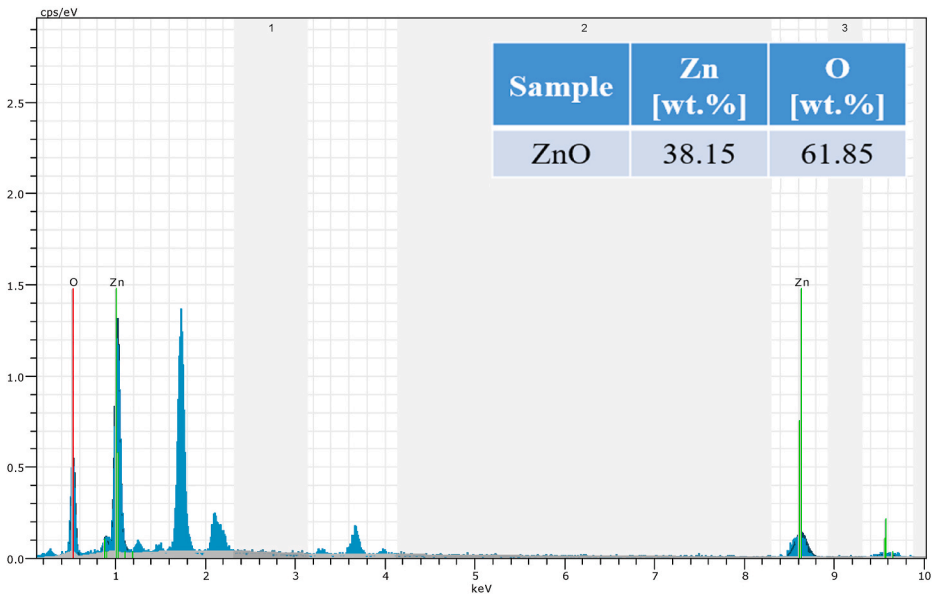

Fig. 4. EDX profile for the ZnO thin film. The presence of Zn and O is confirmed from EDX analysis as displayed in Figure.

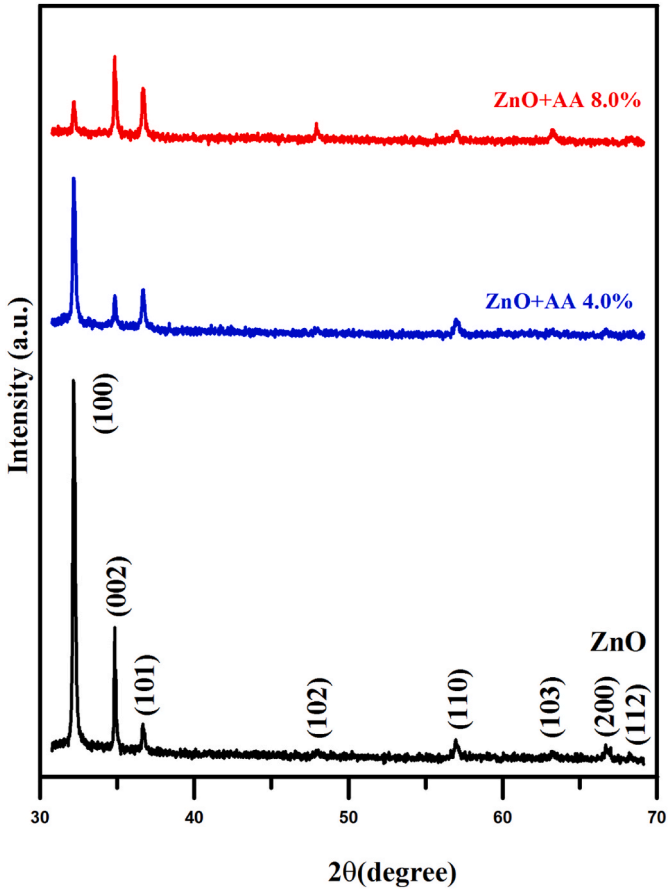

Fig. 5. XRD patterns of ZnO thin films as a function of AA concentrations. It is presented that all the diffraction patterns are good matched with the standard hexagonal wurtzite structure of ZnO. As the concentration of AA was increased from 4.0% to 8.0%, the intensity of the (100) diffraction peak decreased gradually.

Table 1
Crystallite size and film thickness values of green synthesized ZnO samples as a function of AA concentrations.

Sample Name	Crystallite size (nm)	Film Thickness (μm)
ZnO	58.29	0.82
ZnO + AA 4.0%	50.41	0.71
ZnO + AA 8.0%	48.68	0.44

observed that these peaks slightly shifted to higher energy values because of the interactions with the AA. These interactions are more evident in peak intensity, O-H and C-H stretching changes, and bending peaks discussed later. Peaks of ZnO are compatible with the literature, which is prepared by similar methods [9,61–63].

However, the number of peaks occurs when AA is added to the growth solution. From the spectrum of ZnO samples obtained with 4.0% and 8.0% AA, it can be seen that a weak transmittance peak appeared in the range 3217–3730 cm^{-1} created by the OH stretch owing to the presence of moisture in the sample [64,65]. Also, peaks at 2377 cm^{-1} and 2317 cm^{-1} matched with the absorbed atmospheric CO_2 and C=O in acetate moiety [9,66]. Feeble and broadened peaks were observed in the range of 2907–3025 cm^{-1} C–H stretching vibrations. The spectrum's firm absorption peaks at 1745-1570 cm^{-1} have been based on the stretching vibrations of C=O and C=C along with the furanone ring system [64]. Around the short-frequency fingerprint region, bending and wagging bands of C–H are observed in the range 1405-1325 cm^{-1}. The peaks at 1288-1020 cm^{-1} are attributed to characteristic C–O–C and C–O–H bending and stretching vibrations.

At higher frequencies, the characteristic peaks of ZnO were mixed with the vibration peaks of OH out of plane deformations. Moreover, C-H and O-H bending peaks occur at higher energies because of the ZnO-AA interaction. In the presence of a robust intermolecular H bond, the peak intensity tends to decrease [67,68]. In the present study, different from the well-defined examples for AA in the literature, it has been observed that there is a significant decrease in the intensity of the peaks above 2800 cm^{-1} and some shift and peak intensities change at the wavelengths below 1020 cm^{-1}. This type of deformation in some IR peaks indicates the presence of intermolecular hydrogen bonding [69].

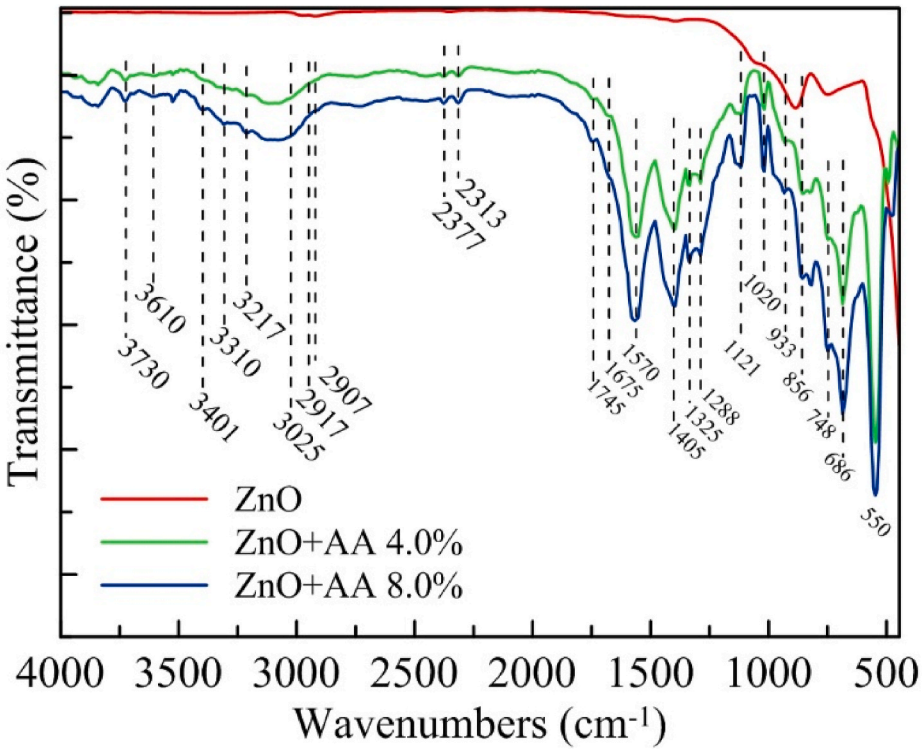

Fig. 6. FTIR spectrums of bare ZnO (−), ZnO+AA 4.0% (−) and ZnO+AA 8.0% (−)thin films. It can be seen that a transmittance peak appeared at about 886 cm^{-1} and 748 cm^{-1} created by the characteristic stretching vibration mode of the Zn–O.

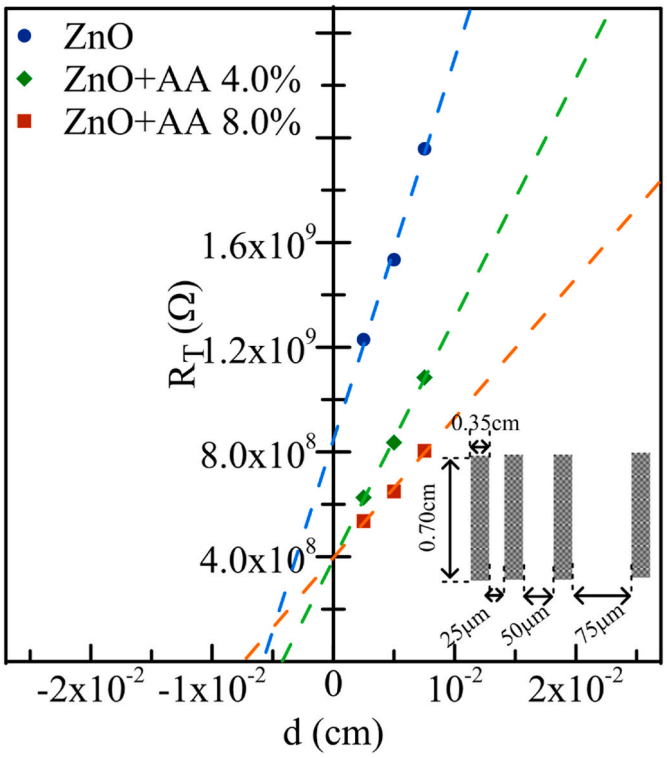

Fig. 7. The total resistance versus gap spacing plots of gold contacts on of bare ZnO, AA 4.0% and AA 8.0% thin films. Resistance values were derived from their I-V characteristics. (For interpretation of the references to colour in this figure legend, the reader is referred to the Web version of this article.)

3.4. Electrical analysis of nanostructured ZnO samples

To take current crowding into account and to be able to extract the specific contact resistivity (ρ_c), contact resistance (R_C), and the transfer length (L_T), the transmission line model (TLM) was used [70,71]. The measurement structure was made on thermally evaporated gold contacts and schematic structure and dimensions given in the inset (Fig. 7). Based on this approach total resistance (R_T) between the pads is described by Ref. [71]:

$$R_T = \frac{2R_{SK}L_T}{w} + \frac{2R_{SH}l}{w} \quad (2)$$

where R_{SK},R_{SH}, l and w, are the sheet resistance under the contact, sheet resistance outside the contact pad width and pad length, respectively. The intercept of calculated total resistance versus gap spacing (d) plot (Fig. 7) is given by $2R_C = \frac{2R_{SK}L_T}{w}$ and can be calculated R_C and L_T values of films (Table 2). By Equation (2), a calculation of ρ_c can be conducted using the L_T, measured from the intersection of the R_T plot for the condition $R_T = 0$ in Fig. 7.

Under the condition $d \gg L_T$, ρ_c can be defined as given below,

$$\rho_c = R_{SH}L_T^2 \quad (3)$$

R_T values of the AA added and bare ZnO films were determined from

Table 2
TLM results of green synthesized ZnO samples as a function of AA concentrations.

Sample Name	R_1 (x$10^9\Omega$)	R_2 (x$10^9\Omega$)	R_3 (x$10^9\Omega$)	L_T (μm)	ρ_c (x$10^6\Omega cm^2$)
ZnO	1.229	1.535	1.957	29.041	0.430
ZnO+AA 4.0%	0.625	0.836	1.085	21.138	0.144
ZnO+AA 8.0%	0.537	0.649	0.803	37.133	0.257

the current-voltage (I–V) measurements. Rectification was not observed in I-V graphs of AA added or bare ZnO films, and the graphics were linear.

As shown in Table 2, the lowest contact resistivity of 0.144 Ωcm^2 was achieved by 4.0% AA. Adding AA in the growth bath slightly reduced the specific contact resistivity, and these values were compatible with films produced by similar methods in the literature [72]. However, the values of ρ_c and L_T were relatively high for all thin films. Both thin films producing method and annealing treatment can be boosting these types' main physical characteristics of obtained nanostructured thin film materials.

3.5. Antibacterial activities of nanostructured ZnO-AA mats

Due to their size, nanoparticles can easily associate with microbial fauna living anywhere. We can use this relationship to our advantage to develop antimicrobial agents. In the study, we tested whether the synthesized ZnO+AA mats have antimicrobial activity. For this purpose, the agar disc diffusion test based on the measurements of the inhibition zones where bacteria could not survive was performed to determine the antimicrobial activity. According to Table 3, ZnO-AA mats are antibacterial against both *E. coli* (ATCC 35218) and *S. aureus* (ATCC 25923). The diameter of the zones of inhibition of 20.1 mm for *E. coli* and 28.1 mm for *S. aureus* at the dose of ZnO+AA is 8.0% (Fig. 8 A.B, e). These inhibition diameters are almost closer or even greater than the diameter of ampicillin, our positive control alone. This proves that the newly synthesized compound is a powerful antibacterial agent. We found that DMSO, which we used as negative control and solvent of synthesized compounds, did not have an antimicrobial effect (Fig. 8 A-B, b). These findings agree with the previous study in our laboratory and other literature [9,36–38].

It was determined that *S. aureus* (ATCC 25923) was more sensitive to ZnO+AA mats than *E. coli (*ATCC 35218), considering the inhibition zones. It is known that gram-positive bacteria are more sensitive to antimicrobial agents than gram-negative bacteria. This is due to the difference in the wall structure of the bacteria. This may explain why gram-positive bacteria with a thick peptidoglycan layer are more exposed to antimicrobial agents [73]. Ascorbic acid had the most substantial effect among boric acid, curcumin, and ascorbic acid used to test its antimicrobial properties against *S. enteritidis* [36]. Likewise, it has been reported that a mixture of nisin, AA, EDTA is effective against *S. enteritidis* ATCC 13076 strain at a dose of 2000 ppm [37]. The chemical characteristic of AA or ascorbate is more anionic and, due to this feature, binds to gram-positive bacteria rather than gram-negative bacteria with a more anionic outer membrane. This feature can explain the more substantial antibacterial effect in gram-positive bacteria. Another study related that the amount of AA in the environment increases the antibacterial activity [74]. Ascorbic acid, which is found in high amounts in the environment, reduces the useable oxygen of the environment because it is a reducing agent. The lack of available oxygen in the environment can have a devastating effect on *S.aureus*, which can grow well in rich oxygen conditions, and *E. coli* which is metabolically versatile. We think that this is the reason for the increased effect at 4.0% and 8.0% concentrations. This finding is consistent with the relevant literature [39]. It is thought that AA alters the outer membrane of bacterial cells, impairing selective permeability, allowing access to target sites of antimicrobial agents [75]. Ascorbic acid in a solution of 1.5% is effective on aerobic bacteria, coliforms, and yeast [38]. Ascorbic acid and lactic acid treatments were applied against *E. coli* O157:H7 strains in food, and it was reported that the 0.4% + 0.2 mixture kept the initial bacterial concentration of 3.98 at 4.12 CFU/ml [39]. Antimicrobial applications of AA have also been mentioned in many other studies [40–43]. The synergistic effect from the antimicrobial agent combination has a greater impact than the individual effect of each antimicrobial agent [52,76–78]. At the same time, the replacement of Zn^{+2} ions leaking into the bacterial culture medium with magnesium ions involved in enzymatic events in bacteria facilitates bacterial death [79]. The destruction of the bacterial cell wall, inhibition of bacterial biochemical activities by leaking compounds, DNA damage and oxidative stress nanoparticles can cause damage to bacteria [80]. It is therefore usual and promising that our combination of ZnO and AA has a higher effect. So far, ZnO mats have been synthesized in many ways and their antimicrobial activities against some bacteria have been tested (Table 4.) [9, 81–89].

Zinc is an essential element for both microorganisms and higher taxa. Also, the association between zinc and immunity is well known. During bacterial infection, host release of Zn^{2+} at mucosal surfaces is an important innate defense mechanism. However, this mechanism has not been fully elucidated. Firstly, manganese is essential for *Staphylococcus* strains growth and its ability to cause disease. Zn^{2+} ions could bind to the manganese transport protein. So, zinc prevented manganese uptake. This slowed bacterial growth and rendered it hypersensitive to immune cell killing [90]. Likewise, bacterial growth cultures also contain manganese. Therefore, this pathway may be a cause of bacterial inhibition. Antibiotics are often ineffective against biofilm-producing bacteria, due to their reduced growth rate and different gene expression [91,92]. Therefore, their synthesis with ZnO mats and Zn^{2+} can eliminate this effect. Ion channels and proton pumps in the cell membrane maintain the membrane potential. It is known that Zn^{2+} depolarizes the membrane potential. Zn^{2+} ions released from ZnO-derived mats increase their concentration in aqueous solutions over time. Ion channels working to maintain the membrane potential will carry the increased Zn^{2+} ions in the extracellular environment into the cell with these pumps step by step. P-type ATPases are enzymes that provide bacterial resistance to heavy metal ions [93]. Zn^{2+} ions transported into the cell inhibit ATP synthesis in this way. Changing the membrane potential and inhibiting the synthesis of ATP, which is used to obtain basic energy, ultimately leads to the death of the bacteria.

The size of the synthesized nanoparticle affects its antimicrobial properties. It has been determined that nanoparticles in the size of 100–800 nm disrupt the wall's integrity by changing the bacterial cell wall [94]. The size of the synthesized nanoparticles is 226–758 nm for bare ZnO, 713–887 nm ZnO+AA 4.0% and 438–1123 nm for ZnO+AA 8.0%. Relatively small particle size increases the effect of antimicrobial agents as they increase the permeation capacity of the bacterial membrane. For the synthesized ZnO+AA nanoparticles, this size is compatible with the size stated in the literature [94]. Fighting resistant bacterial strains that cause loss of life, hospital infections, and great financial losses are among the primary targets of newly synthesized nanoparticles. It is essential to synthesize such cheap, easy and environmentally friendly nanoparticles and increase their usage area in the fight against multi-drug-resistant bacterial strains.

Table 3
Antibacterial activity of nanostructured ZnO + AA mats in the different concentrations, bare ZnO, pure AA and reference antibiotic (ampicillin) against gram-positive and gram-negative bacteria species. The inhibition zone includes a diameter of the disc (6 mm).

	Sample Name	Microorganisms	
		Escherichia coli (gram-negative)	*Staphylococcus aureus* (gram-positive)
Inhibition zone (mm)	ZnO	11.8	11.3
	AA	16.2	25.5
	ZnO+AA 4.0%	17.7	27.8
	ZnO+AA 8.0%	20.1	28.1
	(+) Control, (amp.)	23.8	23.8
	(−) Control 10% DMSO	–	–

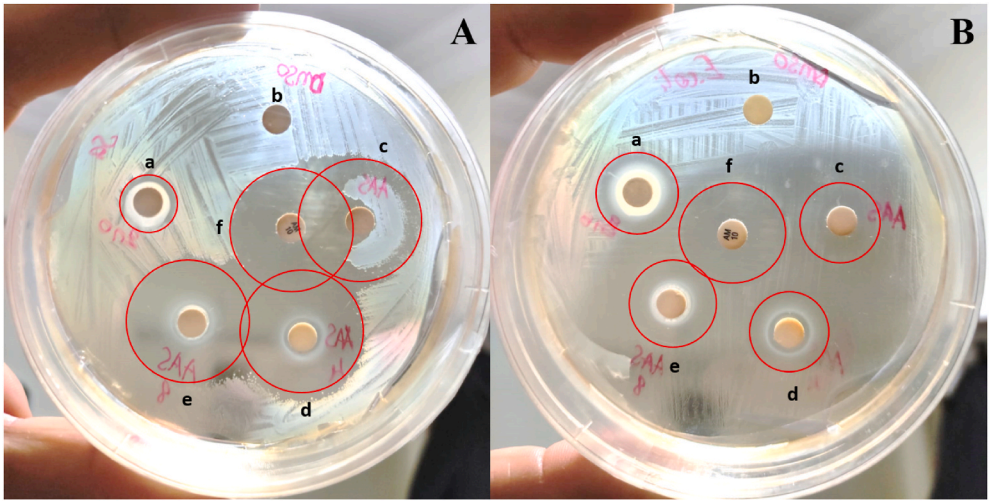

Fig. 8. Antimicrobial effect of synthesized ZnO nanoparticles using ascorbic acid in the different doses. Ampicillin and synthesized ZnO + AA nanoparticles were shown an inhibitory effect on the *Staphylococcus aureus* (A) and *Escherichia* coli (B). Inhibition zones of different diameters were showed in the bare ZnO (a), bare AA (c), ZnO+AA 4.0% (d), ZnO+AA 8.0% (e) and ampicillin as positive control (f). Pure AA extracts and ZnO doped AA have been shown to an inhibitory effect on *Staphylococcus aureus* (A) and *Escherichia coli* (B). On the contrary, inhibition zone of the disc containing 10 μl of the pure DMSO (b) was not shown.
*The red circle to the largest diameter of the zone of inhibition. (For interpretation of the references to colour in this figure legend, the reader is referred to the Web version of this article.)

Table 4
Some selected studies on published about ZnO mats.

Synthesized materials	Antimicrobial activity test methods	Pathogenic microorganisms	Refs.
ZnO+*Vipurnum opulus* (plant extract)	DDM	*Escherichia coli Staphylococcus aureus*	Taşdemir et al., 2021 [9]
ZnO nanotubes	DDM, MIC	*Escherichia coli Staphylococcus aureus Pseudomonas aeruginosa Bacillus subtilis*	Elkady et al., 2015 [81],
ZnO NPs	DDM, SD, MIC	*Klebsiella pneumoniae*	Reddy et al., 2014 [82]
ZnO nanorods	DDM	*Escherichia coli Bacillus subtilis*	Sharma et al., 2012 [83]
ZnO-1,2,3 NPs	DDM, BD, MIC	*Escherichia coli Staphylococcus aureus Pseudomonas aeruginosa Candida albicans*	Pasquet et al., 2014 [84]
ZnO MPs and NPs	DDM	*Enterobacter aerogenes Staphylococcus epidermidis*	Jeyabharathi et al., 2020 [85]
ZnO/TiO_2	DDM, BD; MIC	*Staphylococcus aureus Pseudomonas fluorescens Listeria monocytogenes Escherichia coli*	Azizi-Lalabadi et al., 2019 [86]
C-nZnO composites	DDM, CC	*Escherichia coli Staphylococcus aureus*	Noman and Petru, **2020** [87]
Zinc oxide microparticles loaded cotton (ZOMLC)	DDM	*Escherichia coli*	Bajpai et al., **2011** [88]
Kappa-carrageenan wrapped ZnO NPs	DDM, MIC	*Staphylococcus aureus*	Vijayakumar et al., **2020** [89]

*DDM: Disk diffusion method, MIC: The minimum inhibitory concentration, SD: Serial dilution, BD: Broth dilution CC: Colony counting.

4. Conclusion

In this paper, nanosized ZnO samples were grown by the cost-effective SILAR method, and their main physical characteristics were investigated as a function of AA concentration. Different concentrations of AA (0.0%, 4.0% and 8.0%) influenced the structural, morphological, electrical, and antibacterial properties of nanostructured ZnO materials. The structural and morphological analyses of the samples confirm the structure of beneficial grade ZnO materials with a hexagonal wurtzite structure. The grain sizes and distribution of the particles were modified significantly after AA adding in the starting growth bath. As the concentration of AA was increased from 4.0% to 8.0%, the intensity of the (100) diffraction peak decreased gradually.

Meanwhile, AA concentration increased from 0.0% to 8.0% as the film thickness decreased from 0.82 to 0.44 μm. FTIR transmittance spectra of bare ZnO presented a transmittance peak of about 886 cm^{-1} and 748 cm^{-1} created by the characteristic stretching vibration mode of the Zn-O. It was recorded that these peaks slightly shifted to higher energy values because of the interactions with the AA. The lowest contact resistivity of 0.144 Ωcm^2 was achieved by AA 4.0%. Adding AA in the growth bath slightly reduced the specific contact resistivity, and these values were compatible with films produced by similar methods in the literature. The size of the synthesized nanoparticles was 226–758 nm for bare ZnO, 713–887 nm ZnO+AA 4.0%, and 438–1123 nm for ZnO-+AA 8.0%.

Compared with existing antibiotics, it was observed that the newly synthesized compound showed antibacterial activity with different mechanisms. These mechanisms are physical damage caused by the release of Zn^{+2}, particle absorption, photocatalytic activity depending on the production technique, and ROS production. This bacterial interaction mechanism gives the newly synthesized compounds stronger properties than antibiotics. Also, we observe that, relatively small particle sizes increased the effect of antimicrobial agents as they increased the permeation capacity of the bacterial membrane and synergistic effect from the antimicrobial agent combination has a greater impact than the individual effect of each antimicrobial agent. Thus, AA added ZnO nanostructures could be a cheap, easy and environmentally friendly promising candidate for multiple technological device technology and management of bacterial diseases.

Declaration of competing interest

The authors declare that they have no known competing financial interests or personal relationships that could have appeared to influence the work reported in this paper.

References

[1] M. Darroudi, Z. Sabouri, R. Kazemi Oskuee, A. Khorsand Zak, H. Kargar, M.H. N. Abd Hamid, Green chemistry approach for the synthesis of ZnO nanopowders and their cytotoxic effects, Ceram. Int. 40 (2014) 4827–4831.

[2] S. Rajaboopathi, S. Thambidurai, Synthesis of bio-surfactant based Ag/ZnO nanoparticles for better thermal, photocatalytic and antibacterial activity, Mater. Chem. Phys. 223 (2019) 512–522.

[3] K. Raja, P. Ramesh, D. Geetha, T. Kokila, R. Sathiyapriya, Synthesis of structural and optical characterization of surfactant capped ZnO nanocrystalline, Spectrochim. Acta Mol. Biomol. Spectrosc. 136 (2015) 155–161.

[4] K.Y. Ko, H. Kang, J. Park, B.-W. Min, H.S. Lee, S. Im, J.Y. Kang, J.-M. Myoung, J.-H. Jung, S.-H. Kim, ZnO homojunction core–shell nanorods ultraviolet photo-detecting diodes prepared by atomic layer deposition, Sensor Actuator Phys. 210 (2014) 197–204.

[5] D. Sinar, G.K. Knopf, Disposable piezoelectric vibration sensors with PDMS/ZnO transducers on printed graphene-cellulose electrodes, Sensor Actuator Phys. 302 (2020), 111800.

[6] A. Shah, R.A. Zargar, M. Arora, P. Sundar, Fabrication of pulsed laser-deposited Cr-doped zinc oxide thin films: structural, morphological, and optical studies, J. Mater. Sci. Mater. Electron. 31 (2020) 21193–21202.

[7] C. Kumari, A. Pandey, A. Dixit, Zn interstitial defects and their contribution as efficient light blue emitters in Zn rich ZnO thin films, J. Alloys Compd. 735 (2018) 2318–2323.

[8] S.H. Ribut, C.A.C. Abdullah, M.Z.M. Yusoff, Investigations of structural and optical properties of zinc oxide thin films growth on various substrates, Results Phys. 13 (2019), 102146.

[9] A. Taşdemir, R. Aydın, A. Akkaya, N. Akman, Y. Altınay, H. Çetin, B. Şahin, A. Uzun, E. Ayyildiz, A green approach for the preparation of nanostructured zinc oxide: characterization and promising antibacterial behaviour, Ceram. Int. 47 (2021) 19362–19373.

[10] S.H. Ribut, C.A.C. Abdullah, M. Mustafa, M.Z.M. Yusoff, S.N.A. Azman, Influence of pH variations on zinc oxide nanoparticles and their antibacterial activity, Mater. Res. Express 6 (2018), 025016.

[11] F. Hossein-Babaei, M. Akbari-Saatlu, Growing continuous zinc oxide layers with reproducible nanostructures on the seeded alumina substrates using spray pyrolysis, Ceram. Int. 46 (2020) 8567–8574.

[12] M. Tsega, F.B. Dejene, D.-H. Kuo, Defect related green–red luminescence of Sb-doped ZnO nanorods grown by vapor-phase oxidation method, J. Nanosci. Nanotechnol. 18 (2018) 5785–5789.

[13] H. Waqas, M.S. Salman, A. Riaz, N. Riaz, S. Shabbir, Unique morphologies of zinc oxide synthesized by thermal decomposition and co-precipitation routes: ultraviolet absorption and luminescence characteristics, Cryst. Res. Technol. 50 (2015) 379–388.

[14] A. Dhanalakshmi, S. Thanikaikarasan, B. Natarajan, Influence of Mn dopant concentration on film thickness, structural, morphological, compositional and optical properties of zinc oxide thin films, J. Mater. Sci. Mater. Electron. 28 (2017) 11576–11583.

[15] M. Darroudi, Z. Sabouri, R. Kazemi Oskuee, A. Khorsand Zak, H. Kargar, M.H.N. A. Hamid, Sol–gel synthesis, characterization, and neurotoxicity effect of zinc oxide nanoparticles using gum tragacanth, Ceram. Int. 39 (2013) 9195–9199.

[16] B. Şahin, T. Kaya, Enhanced hydration detection properties of nanostructured CuO films by annealing, Microelectron. Eng. 164 (2016) 88–92.

[17] O. Daoudi, A. Elmadani, M. Lharch, M. Fahoume, A new efficient synthesis of CuO thin films using modified SILAR method, Opt. Quant. Electron. 52 (2020) 1–17.

[18] B. Şahin, R. Aydın, H. Çetin, Variation of the key morphological, structural, optical and electrical properties of SILAR CdO with alkaline earth Ca^{2+} ions doping, Ceram. Int. 45 (2019) 16748–16758.

[19] OECD, Health and Economic Burden of Antimicrobial Resistance, OECD Publishing, Paris, 2019.

[20] M. Institute of, Dietary Reference Intakes for Vitamin C, Vitamin E, Selenium, and Carotenoids, The National Academies Press, Washington, DC, 2000.

[21] M.E. Shils, J.A. Olson, M. Shike, A.C. Ross, K.T.R.L. Olson, P. Ross, M.D.S. Maurice E Shils, Modern Nutrition in Health and Disease: Vitamin C, Williams & Wilkins1999.

[22] C.J. Rebouche, Renal handling of carnitine in experimental vitamin C deficiency, Metabolism 44 (1995) 1639–1643.

[23] I.P. Ronchetti, D. Quaglino, G. Bergamini, Ascorbic acid and connective tissue, in: J.R. Harris (Ed.), Subcellular Biochemistry: Ascorbic Acid: Biochemistry and Biomedical Cell Biology, Springer US, Boston, MA, 1996, pp. 249–264.

[24] H. Katsuki, Vitamin C and nervous tissue in vivo and in vitro aspects, in: J.R. Harris (Ed.), Subcellular Biochemistry: Ascorbic Acid: Biochemistry and Biomedical Cell Biology, Springer US, Boston, MA, 1996, pp. 293–311.

[25] D.F. Horrobin, Ascorbic acid and prostaglandin synthesis, in: J.R. Harris (Ed.), Subcellular Biochemistry: Ascorbic Acid: Biochemistry and Biomedical Cell Biology, Springer US, Boston, MA, 1996, pp. 109–115.

[26] J. Millar, The nitric oxide/ascorbate cycle: how neurones may control their own oxygen supply, Med. Hypotheses 45 (1995) 21–26.

[27] R. Heller, F. Münscher-Paulig, R. Gräbner, U. Till, Ascorbic acid potentiates nitric oxide synthesis in endothelial cells, J. Biol. Chem. 274 (1999) 8254–8260.

[28] J.V. Hirschmann, G.J. Raugi, Adult scurvy, J. Am. Acad. Dermatol. 41 (1999) 895–910.

[29] W.I. El Atrouni, B.M. Knoll, B.D. Lahr, J.E. Eckel-Passow, I.G. Sia, L.M. Baddour, Temporal trends in the incidence of Staphylococcus aureus bacteremia in olmsted county, Minnesota, 1998 to 2005: a population-based study, Clin. Infect. Dis. 49 (2009) e130–e138.

[30] Y. Rhee, A. Aroutcheva, B. Hota, R.A. Weinstein, K.J. Popovich, Evolving epidemiology of Staphylococcus aureus bacteremia, Infect. Control Hosp. Epidemiol. 36 (2015) 1417–1422.

[31] Y.C. Tong Steven, S. Davis Joshua, E. Eichenberger, L. Holland Thomas, G. Fowler Vance, Staphylococcus aureus infections: epidemiology, pathophysiology, clinical manifestations, and management, Clin. Microbiol. Rev. 28 (2015) 603–661.

[32] J. van Hal Sebastian, O. Jensen Slade, L. Vaska Vikram, A. Espedido Björn, L. Paterson David, B. Gosbell Iain, Predictors of mortality in Staphylococcus aureus bacteremia, Clin. Microbiol. Rev. 25 (2012) 362–386.

[33] M. Bonten, J.R. Johnson, A.H.J. van den Biggelaar, L. Georgalis, J. Geurtsen, P.I. de Palacios, S. Gravenstein, T. Verstraeten, P. Hermans, J.T. Poolman, Epidemiology of Escherichia coli bacteremia: a systematic literature review, Clin. Infect. Dis. 72 (2021) 1211–1219.

[34] Eucast, Routine and extended internal quality control for MIC determination and disk diffusion as recommended by EUCAST, Eucast 10 (2020) 1–20.

[35] T.C. Abbey, E. Deak, in: 29th EditionWhat's New from the CLSI Subcommittee on Antimicrobial Susceptibility Testing M100, vol. 41, Clinical Microbiology Newsletter, 2019, pp. 203–209.

[36] D. Hernandez-Patlan, B. Solis-Cruz, A. Méndez-Albores, J.D. Latorre, X. Hernandez-Velasco, G. Tellez, R. López-Arellano, Comparison of PrestoBlue® and plating method to evaluate antimicrobial activity of ascorbic acid, boric acid and curcumin in an in vitro gastrointestinal model, J. Appl. Microbiol. 124 (2018) 423–430.

[37] N. Sangcharoen, W. Klaypradit, P. Wilaipun, Antimicrobial activity optimization of nisin, ascorbic acid and ethylenediamine tetraacetic acid disodium salt (EDTA) against Salmonella Enteritidis ATCC 13076 using response surface methodology, Agricult. Nat. Resour. 51 (2017) 355–364.

[38] J.Z. Acedo, D.A.C. Varron, I.C. Emnace, R.D. Lauzon, A.L. Acedo Jr., Antimicrobial effects of ascorbic acid and calcium lactate, in: Freshcut Jackfruit (*Artocarpus Heterophyllus* Lam.), International Society for Horticultural Science (ISHS), Leuven, Belgium, 2013, pp. 199–208.

[39] M. Tajkarimi, S.A. Ibrahim, Antimicrobial activity of ascorbic acid alone or in combination with lactic acid on Escherichia coli O157:H7 in laboratory medium and carrot juice, Food Control 22 (2011) 801–804.

[40] A. Popelka, A. Abdulkareem, A.A. Mahmoud, M.G. Nassr, M.K.A.A. Al-Ruweidi, K. J. Mohamoud, M.K. Hussein, M. Lehocky, D. Vesela, P. Humpolíček, P. Kasak, Antimicrobial modification of PLA scaffolds with ascorbic and fumaric acids via plasma treatment, Surf. Coating. Technol. 400 (2020), 126216.

[41] N.M. Zain, A.G.F. Stapley, G. Shama, Green synthesis of silver and copper nanoparticles using ascorbic acid and chitosan for antimicrobial applications, Carbohydr. Polym. 112 (2014) 195–202.

[42] A. Fite, R. Dykhuizen, A. Litterick, M. Golden, C. Leifert, Effects of ascorbic acid, glutathione, thiocyanate, and iodide on antimicrobial activity of acidified nitrite, Antimicrob. Agents Chemother. 48 (2004) 655–658.

[43] M. Stevanović, I. Bračko, M. Milenković, N. Filipović, J. Nunić, M. Filipič, D. P. Uskoković, Multifunctional PLGA particles containing poly(l-glutamic acid)-capped silver nanoparticles and ascorbic acid with simultaneous antioxidative and prolonged antimicrobial activity, Acta Biomater. 10 (2014) 151–162.

[44] H.N. Sheikh, H. Khajuria, J. Ladol, R. Singh, s. khajuria, Surfactant Assisted Sonochemical Synthesis and Characterization of Gadolinium Doped Zinc Oxide Nanoparticles, vol. 62, 2015, p. 10, 2015.

[45] N. Singh, S. Mittal, K. Sood, P. Gupta, Controlling the flow of nascent oxygen using hydrogen peroxide results in controlling the synthesis of ZnO/ZnO_2, Chalcogenide Lett. 7 (2010).

[46] S. Ashok Kumar, H.-W. Cheng, S.-M. Chen, Electroanalysis of ascorbic acid (vitamin C) using nano-ZnO/poly(luminol) hybrid film modified electrode, React. Funct. Polym. 69 (2009) 364–370.

[47] A. Akkaya, E. Ayyıldız, Automation software for semiconductor research laboratories: electrical parameter calculation program (SeCLaS-PC), J. Circ. Syst. Comput. 29 (2020), 2050215.

[48] A. Akkaya, E. Ayyıldız, Automation software for semiconductor research laboratories: measurement system and instrument control program (SeCLaS-IC), MAPAN 35 (2020) 343–350.

[49] S. Cho, H. Jeong, D.-H. Park, S.-H. Jung, H.-J. Kim, K.-H. Lee, The effects of vitamin C on ZnO crystal formation, CrystEngComm 12 (2010) 968–976.

[50] N. Chaithanatkun, D. Chantarawong, P. Songkeaw, K. Onlaor, T. Thiwawong, B. Tunhoo, Effect of ascorbic acid on structural properties of ZnO nanoparticles prepared by precipitation process, in: 10th IEEE International Conference on Nano/Micro Engineered and Molecular Systems, IEEE, 2015, pp. 145–148.

[51] W. Long, L. Fu, Hydrothermal synthesis of ZnO flower-reduced graphene oxide composite for electrochemical determination of ascorbic acid, Fullerenes, Nanotub. Carbon Nanostruct. 25 (2017) 404–409.

[52] B. Şahin, S. Soylu, M. Kara, M. Türkmen, R. Aydin, H. Çetin, Superior antibacterial activity against seed-borne plant bacterial disease agents and enhanced physical properties of novel green synthesized nanostructured ZnO using Thymbra spicata plant extract, Ceram. Int. 47 (2021) 341–350.

[53] V.R. Chelli, A.K. Golder, Ag-doping on ZnO support mediated by bio-analytes rich in ascorbic acid for photocatalytic degradation of dipyrone drug, Chemosphere 208 (2018) 149–158.

[54] M. Kumar, B.K. Swamy, S. Reddy, T. Sathisha, J. Manjanna, Synthesis of ZnO and its surfactant based electrode for the simultaneous detection of dopamine and ascorbic acid, Anal Methods-Uk 5 (2013) 735–740.

[55] E. Gürbüz, R. Aydin, B. Şahin, A study of the influences of transition metal (Mn,Ni) co-doping on the morphological, structural and optical properties of nanostructured CdO films, J. Mater. Sci. Mater. Electron. 29 (2018) 1823–1831.

[56] B.D. Cullity, Elements of X-ray diffraction, Am. J. Phys. 25 (1957) 394–395.

[57] P. Scherrer, Bestimmung der Grösse und der inneren Struktur von Kolloidteilchen mittels Röntgenstrahlen, Nachr. Ges. Wiss. Göttingen (1918) 98–100.
[58] L. Al-Salem, R. Seoudi, Influence of ascorbic acid as modifier on the particle size and the optical properties of ZnO nanoparticles, J. Mater. Sci. Mater. Electron. 31 (2020) 22642–22651.
[59] S. Sagadevan, S. Vennila, A.R. Marlinda, Y. Al-Douri, M.R. Johan, J.A. Lett, Synthesis and evaluation of the structural, optical, and antibacterial properties of copper oxide nanoparticles, Appl. Phys. A 125 (2019) 1–9.
[60] A. Abedini, A.R. Daud, M.A. Abdul Hamid, N. Kamil Othman, E. Saion, A review on radiation-induced nucleation and growth of colloidal metallic nanoparticles, Nanoscale Res. Lett. 8 (2013) 474.
[61] N. Rao, M. Rao, Structural and optical investigation of ZnO nanopowders synthesized from zinc chloride and zinc nitrate, Am. J. Mater. Sci. 5 (2015) 66–68.
[62] M. Sathya, A. Claude, P. Govindasamy, K. Sudha, A. Claude, Growth of pure and doped ZnO thin films for solar cell applications, Adv. Appl. Sci. Res. 3 (2012) 2591–2598.
[63] A. Akkaya, B. Şahin, R. Aydın, H. Çetin, E. Ayyıldız, Solution-processed nanostructured ZnO/CuO composite films and improvement its physical properties by lustrous transition metal silver doping, J. Mater. Sci. Mater. Electron. 31 (2020) 14400–14410.
[64] C.Y. Panicker, H.T. Varghese, D. Philip, FT-IR, FT-Raman and SERS spectra of Vitamin C, Spectrochim. Acta Mol. Biomol. Spectrosc. 65 (2006) 802–804.
[65] K.R. Ahammed, M. Ashaduzzaman, S.C. Paul, M.R. Nath, S. Bhowmik, O. Saha, M. M. Rahaman, S. Bhowmik, T.D. Aka, Microwave assisted synthesis of zinc oxide (ZnO) nanoparticles in a noble approach: utilization for antibacterial and photocatalytic activity, SN Appl. Sci. 2 (2020) 1–14.
[66] G. Richner, G. Puxty, Assessing the chemical speciation during CO_2 absorption by aqueous amines using in situ FTIR, Ind. Eng. Chem. Res. 51 (2012) 14317–14324.
[67] S. Burikov, T. Dolenko, S. Patsaeva, Y. Starokurov, V. Yuzhakov, Raman and IR spectroscopy research on hydrogen bonding in water–ethanol systems, Mol. Phys. 108 (2010) 2427–2436.
[68] B. Athokpam, S.G. Ramesh, R.H. McKenzie, Effect of hydrogen bonding on the infrared absorption intensity of OH stretch vibrations, Chem. Phys. 488–489 (2017) 43–54.
[69] A.V. Stuart, G.B.B.M. Sutherland, Effect of hydrogen bonding on the deformation frequencies of the hydroxyl group in alcohols, J. Chem. Phys. 24 (1956) 559–570.
[70] D.K. Schroder, Semiconductor Material and Device Characterization, John Wiley & Sons, New York, 2006.
[71] G.K. Reeves, H.B. Harrison, Obtaining the specific contact resistance from transmission-line model measurements, Electron Devic Lett 3 (1982) 111–113.
[72] I. Karaduman Er, İ.A. Yıldız, T. Bayraktar, S. Acar, A. Ateş, The dependence of the gas sensing properties of ZnO thin films on the zinc concentration, J. Mater. Sci. Mater. Electron. 32 (2021) 8122–8135.
[73] A. Mai-Prochnow, M. Clauson, J. Hong, A.B. Murphy, Gram positive and Gram negative bacteria differ in their sensitivity to cold plasma, Sci Rep-Uk 6 (2016), 38610.
[74] B.M. Abu-Ghazaleh, Inhibition of Citrobacter freundii by lactic acid, ascorbic acid, citric acid,Thymus vulgaris extract and NaCl at 31°C and 5°C, Ann. Microbiol. 56 (2006) 261.
[75] T.E. Miller, Killing and lysis of gram-negative bacteria through the synergistic effect of hydrogen peroxide, ascorbic acid, and lysozyme, J. Bacteriol. 98 (1969) 949–955.
[76] R.J.W. Lambert, M.D. Johnston, G.W. Hanlon, S.P. Denyer, Theory of antimicrobial combinations: biocide mixtures – synergy or addition? J. Appl. Microbiol. 94 (2003) 747–759.
[77] M. Alkasir, N. Samadi, Z. Sabouri, Z. Mardani, M. Khatami, M. Darroudi, Evaluation cytotoxicity effects of biosynthesized zinc oxide nanoparticles using aqueous Linum Usitatissimum extract and investigation of their photocatalytic activityackn, Inorg. Chem. Commun. 119 (2020), 108066.
[78] S. Nemati, H.A. Hosseini, A. Hashemzadeh, M. Mohajeri, Z. Sabouri, M. Darroudi, R. Kazemi Oskuee, Cytotoxicity and photocatalytic applications of biosynthesized ZnO nanoparticles by Rheum turketanicum rhizome extract, Mater. Res. Express 6 (2019), 125016.
[79] S. Tavassoli Hojati, H. Alaghemand, F. Hamze, F. Ahmadian Babaki, R. Rajab-Nia, M.B. Rezvani, M. Kaviani, M. Atai, Antibacterial, physical and mechanical properties of flowable resin composites containing zinc oxide nanoparticles, Dent. Mater. 29 (2013) 495–505.
[80] A. Besinis, T. De Peralta, R.D. Handy, The antibacterial effects of silver, titanium dioxide and silica dioxide nanoparticles compared to the dental disinfectant chlorhexidine on Streptococcus mutans using a suite of bioassays, Nanotoxicology 8 (2014) 1–16.
[81] M.F. Elkady, H. Shokry Hassan, E.E. Hafez, A. Fouad, Construction of zinc oxide into different morphological structures to Be utilized as antimicrobial agent against multidrug resistant bacteria, Bioinorgan. Chem. Appl. (2015), 536854, 2015.
[82] L.S. Reddy, M.M. Nisha, M. Joice, P.N. Shilpa, Antimicrobial activity of zinc oxide (ZnO) nanoparticle against Klebsiella pneumoniae, Pharm. Biol. 52 (2014) 1388–1397.
[83] S. Sharma, D. Naik, V. Agarwala, Synthesis, characterization and antibacterial activity of ZnO nanoparticles of different morphology, Adv. Mater. Res. 585 (2012) 154–158.
[84] J. Pasquet, Y. Chevalier, E. Couval, D. Bouvier, G. Noizet, C. Morlière, M.-A. Bolzinger, Antimicrobial activity of zinc oxide particles on five micro-organisms of the Challenge Tests related to their physicochemical properties, Int. J. Pharm. 460 (2014) 92–100.
[85] S. Jeyabharathi, R. Mahalakshmi, S. Chandramohan, S. Naveenkumar, K. Sundar, A. Muthukumaran, Self-assembled hollow ZnO nano and micro donut shape by starch and its antimicrobial potentials, Mater. Lett. 275 (2020), 128128.
[86] M. Azizi-Lalabadi, A. Ehsani, B. Divband, M. Alizadeh-Sani, Antimicrobial activity of Titanium dioxide and Zinc oxide nanoparticles supported in 4A zeolite and evaluation the morphological characteristic, Sci Rep-Uk 9 (2019), 17439.
[87] M.T.T. Noman, M. Petrů, Functional properties of sonochemically synthesized zinc oxide nanoparticles and cotton composites, Nanomater. Basel 10 (2020) 1661.
[88] S.K. Bajpai, V. Thomas, M. Bajpai, Novel strategy for synthesis of ZnO microparticles loaded cotton fabrics and investigation of their antibacterial properties, J. Eng. Fiber Fabrics 6 (2011), 155892501100600310.
[89] S. Vijayakumar, K. Saravanakumar, B. Malaikozhundan, M. Divya, B. Vaseeharan, E.F. Durán-Lara, M.-H. Wang, Biopolymer K-carrageenan wrapped ZnO nanoparticles as drug delivery vehicles for anti MRSA therapy, Int. J. Biol. Macromol. 144 (2020) 9–18.
[90] C.A. McDevitt, A.D. Ogunniyi, E. Valkov, M.C. Lawrence, B. Kobe, A.G. McEwan, J. C. Paton, A molecular mechanism for bacterial susceptibility to zinc, PLoS Pathog. 7 (2011), e1002357.
[91] M.C. Sánchez, P. Romero-Lastra, H. Ribeiro-Vidal, A. Llama-Palacios, E. Figuero, D. Herrera, M. Sanz, Comparative gene expression analysis of planktonic Porphyromonas gingivalis ATCC 33277 in the presence of a growing biofilm versus planktonic cells, BMC Microbiol. 19 (2019) 58.
[92] O. Besharova, V.M. Suchanek, R. Hartmann, K. Drescher, V. Sourjik, Diversification of gene expression during formation of static submerged biofilms by Escherichia coli, Front. Microbiol. 7 (2016).
[93] W. Fan, Q. Sun, Y. Li, F.R. Tay, B. Fan, Synergistic mechanism of Ag^{+}–Zn^{2+} in antibacterial activity against Enterococcus faecalis and its application against dentin infection, J. Nanobiotechnol. 16 (2018) 10.
[94] O. Yamamoto, Influence of particle size on the antibacterial activity of zinc oxide, Int. J. Inorg. Mater. 3 (2001) 643–646.